Control Engineering Practice 20 (2012) 465–476

Contents lists available at SciVerse ScienceDirect

Control Engineering Practice

journal homepage: www.elsevier.com/locate/conengprac

Model predictive control of dissolved oxygen concentration based on a self-organizing RBF neural network ☆

Hong-Gui Han *, Jun-Fei Qiao, Qi-Li Chen

College of Electronic and Control Engineering, Beijing University of Technology, Beijing, China

ARTICLE INFO

Article history:
Received 17 June 2011
Accepted 7 January 2012
Available online 20 January 2012

Keywords:
Dissolved oxygen concentration control
Self-organizing radial basis function
Model predictive control
Wastewater treatment process
Benchmark simulation model 1

ABSTRACT

The dissolved oxygen (DO) concentration in activated sludge wastewater treatment processes (WWTPs) is difficult to control because of the complex nonlinear behavior involved. In this paper, a self-organizing radial basis function (RBF) neural network model predictive control (SORBF-MPC) method is proposed for controlling the DO concentration in a WWTP. The proposed SORBF can vary its structure dynamically to maintain prediction accuracy. The hidden nodes in the RBF neural network can be added or removed on-line based on node activity and mutual information (MI) to achieve the appropriate network complexity and the necessary dynamism. Moreover, the convergence of the SORBF is analyzed in both the dynamic process phase and the phase following the modification of the structure. Finally, the SORBF-MPC is applied to the Benchmark Simulation Model 1 (BSM1) WWTP to maintain the DO concentration. The results show that SORBF-MPC effectively provides process control. The performance comparison also indicates that the proposed model's predictive control strategy yields the most accurate for DO concentration, better effluent qualities, and lower average aeration energy (AE) consumption.

1. Introduction

Water pollution is one of the most serious environmental problems due to the discharge of nutrients into receiving waters (Zhang & Hoo, 2008). The most popular treatment method used in wastewater plants is biological processing (Shannon et al., 2008). More specifically, processes based on activated sludge technology represent an excellent method of removing pollution from wastewater. However, the complexity of the physical, chemical, and biological phenomena associated with treatment units means that the performance of the process depends heavily on environmental and operational conditions. It is difficult to control wastewater treatment processes (WWTPs) because of the large disturbances in flow and load and the different physical and biological phenomena at play. Moreover, the reactors exhibit common features of industrial systems, such as nonlinear dynamics and coupling effects among the variables (Wahaba, Katebia, & Balderud, 2009; Chachuat, Roche, & Latifi, 2005; Holenda, Domokos, Redey, & Fazakas, 2007). It is therefore important to study methods of controlling WWTPs.

Today, dissolved oxygen (DO) concentration control is the most widely used method. Oxygen is a key substrate; thus, monitoring its consumption is one of the most effective methods of monitoring the treatment process (Shen, Chen, & Corriou, 2008). The DO level in an aerobic reactor will influence the behavior and activity of the heterotrophic and autotrophic microorganisms living in the activated sludge. The DO concentration during the activated sludge process should be high enough to supply sufficient oxygen to the microorganisms in the sludge and thus degrade the organic substances and convert ammonium into nitrate. However, an excessively high level of DO, which requires a high air inflow rate, will lead to a high level of energy consumption and may lower the sludge quality. Research shows that a high level of DO in internally recirculated water also decreases the efficiency of the de-nitrification process (Shen et al., 2008). Hence, from both an economic and a processing perspective, it is important to control the DO concentration.

Significant research has studied methods of controlling DO as a means to improve the process. The traditional methods referred to as the Proportional–Integral (PI) (Carlsson, Lindberg, Hasselblad, & Xu, 1994) and Proportional–Integral–Derivative (PID) (Carlsson & Rehnstrom, 2002) techniques have been employed extensively.

☆This work was supported by the National Science Foundation of China under Grants 61034008 and 60873043, Beijing Municipal Natural Science Foundation under Grant 4122006 and 4092010, Beijing Municipal Education Commission Science and Technology Development Program (KZ201010005005), Funding Project for Academic Human Resources Development under Grant PHR(IHLB)201006103, New Century Excellent Talents Program from Ministry of Education under Grant NCET-08-0616.

* Corresponding author.
E-mail addresses: Rechardhan@sina.com (H.-G. Han), isibox@sina.com (J.-F. Qiao), shuang3045@163.com (Q.-L. Chen).

0967-0661/$ - see front matter © 2012 Elsevier Ltd. All rights reserved.
doi:10.1016/j.conengprac.2012.01.001

However, due to the nonlinear characteristics of the bioprocesses and the non-existence of adequate hard or soft sensors, the controllers were developed for specific operating and environmental conditions. For these purposes, researchers have recently begun employing artificial intelligence techniques that are also used in a wide variety of applications, including chemicals, automation, and other complex nonlinear systems. The most popular artificial intelligence techniques used to control DO concentration are fuzzy and neural networks (Kruszewski, Wang, & Guerra, 2008). Ferrer, Rodrigo, Seco, and Penyaroja (1998) studied a fuzzy approach to DO control in the aeration process. The inputs to the fuzzy controller are the actual DO concentration, the error value, the error change and the accumulated error; the outputs are the air flow and the change in that value. Compared with conventional on/off controls, a fuzzy controller can save energy. Traore et al. (2005) presented a fuzzy logic strategy for controlling DO levels in a sequential batch reactor (SBR) pilot plant. The strategy was shown to be both robust and effective, and it was also easy to integrate into a global cost management monitoring system. Although the fuzzy approach has been successful in many practical contexts, there is still no clear and easy design methodology, mainly because a fuzzy control rule base is semi-empirical rather than learning. Consequently, a neural network that is able to learn the nonlinear functional relationships involved in the process has become popular. Syu and Chen (1998) have proposed an adaptive control for DO concentration in the sewage treatment process using a backpropagation (BP) neural network. The control system designed sets the minimum dose of hydrogen peroxide and ferrous chloride for performance indicators and the effluent chemical oxygen demand (COD) necessary to meet the emission targets. Lee, Lee, Park, and Park (2005) have developed an automatic control system using a neural network and an internet-based remote monitoring system. It increases the operating efficiency of plants that exhibit serious influent loading variance. The results show that regardless of the loading variance, more than 95% of organic matter and more than 60% of nitrogen and phosphorus are removed. Huang et al. (2009) proposed an integrated neural-fuzzy process controller that could be used to control aeration for DO concentration. It was shown that operational cost savings of almost 30% accrued when the fuzzy neural controller was switched on. There are other neural network-based approaches to controlling DO concentration (Zarrad, Harmand, Devisscher, & Steyer, 2004; Azwar, Rashid, & Hussain, 2008). However, it is difficult for designers and technical experts to estimate all of the input–output data within such a complex system and thus to determine the appropriate structure for the controller's neural network.

Model predictive control (MPC) is widely used in the industry in general and process industries in particular. Holenda, Domokos, Redey, and Fazakas (2008) have proposed an MPC method for determining DO concentration. However, their work was focused on DO control rather than multivariable control. To keep the quality of the effluent within regulated limits, Shen, Chen, Pons, and Corriou (2009) implemented the MPC strategy with the Benchmark Simulation Model 1 (BSM1) for WWTPs. Feedback via linear dynamic matrix control, quadratic dynamic matrix control, and nonlinear MPC has been discussed, as have improvements via feedforward based on the influent flow rate and the ammonium concentration. Acceptable performance is obtained by combining the feedforward controllers and taking into consideration the influent ammonium concentration and the flow rate. However, in some cases in which the influent ammonium concentration is not measured, its estimation requires an observer. Recently, O'Brien et al. investigated a case study application of MPC in which the technique was used in a WWTP in Lancaster, North England. The control system was implemented in real time together with a plant monitoring system for the purpose of process supervision. The MPC system provided significant benefits, including a reduction of more than 25% in power usage and a similar increase in plant efficiency. However, an analysis of the operational data indicated that the DO sensors frequently provided incorrect process measurements in this case study (O'Brien, Mack, Lennox, Lovett, & Wall, 2011). Artificial neural networks (ANNs), originally inspired by the ability of human beings to perform many complicated tasks with ease, are usually used to model complex relationships between inputs and outputs. There are different types of ANNs used in both academic and industrial sectors. The types of networks include radial basis function (RBF) neural networks (Wu, Zhu, Cao, & Tu, 2008), feedforward neural networks (FNNs), and dynamic neural networks (Yüzgeç, Becerikli, & Türker, 2008). However, only the parameters of these models are changed; the structures themselves are not. A new method of adapting RBF network models is developed in this paper. The method can be used to change both the network structure (the number of hidden nodes) and the parameters (the weights). This characteristic makes the method ideal for complex nonlinear dynamic applications. It is reasonable to suppose that RBF design algorithms with adaptive structures will exhibit better performance. In this paper, a new structure-adjusting strategy is developed that is applicable to both constructing and pruning. The unique full structural optimization process is intended to optimize the entire RBF structure using an approach that combines error reparation (ER) with the activity of the hidden nodes. The mutability of the proposed neural network can be used to achieve a compact structure size on-line based on the characteristics of the WWTPs. The SORBF-MPC technology improves the performance of the controller in several key respects in terms of its response, accuracy, and robustness. To demonstrate the efficiency of the proposed strategy, this paper applies the SORBF-MPC to the BSM1 and shows how it is able to improve the control performance of the DO concentration, the quality of the effluent and the average aeration energy (AE) consumption.

This paper is organized as follows: Section 2 briefly discusses the SORBF-MPC design. Section 3 discusses the convergence of the proposed SORBF-MPC method. The results of the simulations (based on the activated sludge system model – BSM1 (Jeppsson & Pons, 2004)) are presented in Section 4. The performance of the SORBF-MPC method is compared with that of several other methods. The results obtained using SORBF-MPC in BSM1 demonstrate that the proposed SORBF-MPC control strategy is efficient – it ensures that the effluent meets the relevant standards and lower the AE consumption. Finally, Section 5 concludes the paper.

For the sake of convenience, Table 1 lists the acronyms used in this paper.

2. Scheme of self-organizing RBF neural network model predictive control (SORBF-MPC)

2.1. Model predictive control (MPC)

The MPC feedback system used in this paper is shown in Fig. 1.

In Fig. 1, r, y, u, and $\hat{y}$ represent the reference variable, control variable, manipulated variable, and predicted outputs, respectively; d is the disturbance, and e_p is the error that indicates the distinction between the process and the prediction model.

For any assumed set of present and future control moves $\Delta u(t)$, $\Delta u(t+1)$, …, $\Delta u(t+H_u-1)$, the future behavior of the process outputs $\hat{y}(t+1|\,t)$, $\hat{y}(t+2|\,t)$, …, $\hat{y}(t+H_p|\,t)$ can be predicted over a horizon H_p. The prediction horizon H_p and control prediction horizon H_u ($H_u < H_p$) are computed to minimize an objective

Table 1
Lists of acronyms.

Acronym	Description
AE	Average aeration energy
AF	Active firing
ANNs	Artificial neural networks
ASM1	Activated sludge model 1
BOD_5	Biological oxygen demand over a 5-day period
BP	Backpropagation
BSM1	Benchmark simulation model 1
COD	Chemical oxygen demand
DO	Dissolved oxygen
ER	Error reparation
FNNs	Feedforward neural networks
GGAP-RBF	Growing and pruning algorithm for RBF
MI	Mutual information
MISO	Multi-input and single-output
MLP	Multi-layer perceptron
MPC	Model predictive control
MPID	Multivariable PID
MRAN	Minimal resources-allocating network
MSE	Mean square error
N_{tot}	Total nitrogen
NARX	Nonlinear autoregressive exogenous
NH	Ammonium
IAE	Integrated absolute error
IAWQ-ASM1	International association on water quality activated sludge model 1
PI	Proportional-integral
PID	Proportional-integral-derivative
RBF	Radial basis function
RBFNN	RBF neural network
SBR	Sequential batch reactor
SORBF	Self-Organizing RBF
SORBF-MPC	Self-Organizing RBF neural network model predictive control
SS	Suspended solids
WWTP	Wastewater treatment process
WWTPs	Wastewater treatment processes

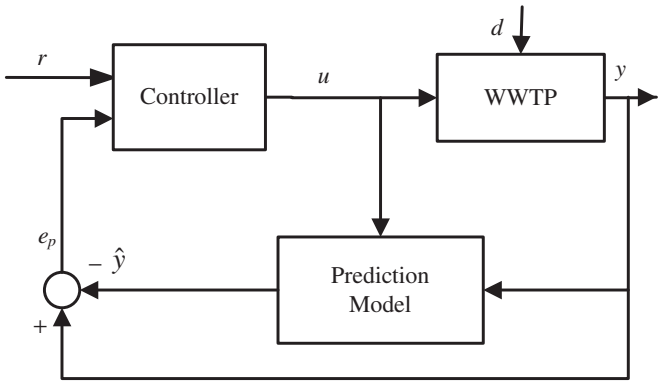

Fig. 1. MPC feedback system.

function J of the form

$$J=\sum_{i=1}^{H_p}[r(t+i)-\hat{y}(t+i)]^T W_i^y[r(t+i)-\hat{y}(t+i)] + \sum_{j=1}^{H_u}\Delta u(t+j-1)^T W_j^u \Delta u(t+j-1), \quad (1)$$

subject to

$$|\Delta u(t)| \le \Delta u_{\max},$$
$$u_{\min} \le u(t) \le u_{\max},$$
$$\hat{y}_{\min} \le \hat{y}(t) \le \hat{y}_{\max}, \quad (2)$$

where W_i^y and W_i^u are the weighting parameters, H_p represents the prediction horizon and H_u is the control prediction horizon. In this study, the DO concentration in the fifth unit is considered the plant output (y) – the control variable – whereas the manipulated variables (u) are the internal flow recirculation (Q_a, (m^3/day)) and the oxygen mass transfer coefficient (K_La, (day^{-1})), $u=[Q_a, K_La]$.

In modeling a dynamic system, the WWTP system as shown in Fig. 1 can be represented as a nonlinear autoregressive exogenous (NARX) model of the following form (Wu et al., 2008)

$$y(t)=h(y(t-1),\ \ldots\ ,y(t-n_y),u(t-1),\ \ldots\ ,u(t-n_u-t_d))+\hbar(t), \quad (3)$$

where $u(t)=[Q_a(t), K_La(t)]$ and $y(t)$ denote the process input and output, $\hbar(t)$is the noise. $y\in\Re$, the function $h(\ )$ is assumed to be unknown, n_y and n_u are the maximum lags in the outputs and inputs, and t_d is the delay time. In this paper, the WWTP that includes influent loads, test procedures, and evaluation criteria is the BSM1, which has been proposed within the framework of COST Actions 682 and 624 (Jeppsson & Pons, 2004).

2.2. RBF neural network modeling

In Fig. 2, the structure of the basic RBF neural network (RBFNN) contains one input layer, one output layer, and one hidden layer. Because the RBFNN is used for a multi-input–single-output (MISO) system in this paper, a MISO RBFNN is selected to better illustrate the SORBF-MPC method.

A single-output RBFNN with K hidden layer nodes can be described by

$$\hat{y}=\sum_{k=1}^{K} w_k\theta_k(\mathbf{x}), \quad (4)$$

where $\mathbf{x}$ and $\hat{y}$ denote the input and output of the network, $\mathbf{x}(t)=[y(t-1),\ \ldots,\ y(t-n_y),\ u(t-1-t_d),\ldots,\ u(t-n_u-t_d)]^T$, w_k is the connecting weights between kth hidden node and the output layer, θ_k is the output value of the kth hidden node, and

$$\theta_k(\mathbf{x})=e^{(-\|\mathbf{x}-\boldsymbol{\mu}_k\|/\sigma_k^2)}, \quad (5)$$

$\boldsymbol{\mu}_k$ denotes the center vector of the kth hidden node, and $\|\mathbf{x}-\boldsymbol{\mu}_k\|$ is the Euclidean distance between $\mathbf{x}$ and $\boldsymbol{\mu}_k$. σ_k is the radius or the width of the kth hidden node.

The RBFNN can be used to predict the process output. In the design of a process controller, the output of the RBFNN can be also shown in the following form

$$\hat{y}(t)=\varphi(\mathbf{x}(t)), \quad (6)$$

where $\varphi(\cdot)$ is a vector-valued nonlinear function. Then, this neural model can be used for control simulation and on-line implementation.

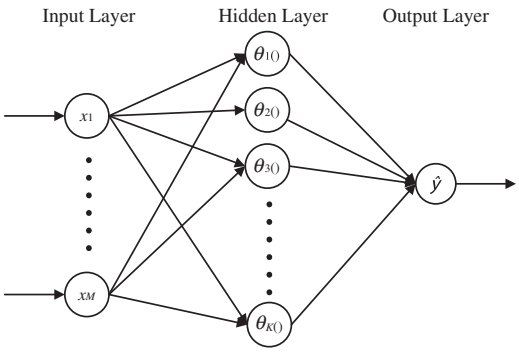

Fig. 2. The RBFNN structure.

2.3. Self-organizing RBF neural network (SORBF)

It is clear that the success of MPC is highly dependent on the existence of a reliable system model. The system model must effectively describe the nonlinear behavior of the system and be easily usable in designing a MPC algorithm. To cope with the changing characteristics of the system, the structure of the RBFNN can be adapted and the weight parameters updated to model time varying dynamics or uncertainty. The SORBF maintains modeling accuracy during adaptation, thus improving control performance.

The SORBF proposed in this paper relies mainly on both the average firing rate of the hidden nodes and the mutual information (MI) intensities of the hidden layer and the output layer. First, the activities of the hidden nodes are evaluated according to the average firing (AF) rate. The hidden nodes that have a high firing rate are divided into new nodes. Then, the MI value is used to adjust the network structure, i.e., the value of the MI is used as a measure of the connectivity between the hidden layer and the output layer. Connections that have a small MI value will be pruned to simplify the structure of the RBFNN. Finally, the gradient-descent method, which is used to adjust the values of the parameters, ensures the precision of the SORBF. Two aspects of the flexible method used to design the structure of the RBFNN will be discussed here: the node-splitting mechanism and the node-adjusting mechanism used to design the structure.

Case 1. Node-Splitting Mechanism

Consider the AF of the hidden nodes described by the following equation

$$Af_i = \frac{1}{\|\mathbf{x}-\boldsymbol{\mu}_i\|+\tau}\frac{\theta_i(\mathbf{x})}{\sum_{i=1}^{K}\theta_i(\mathbf{x})}, \quad (i=1,2,\ldots,K), \tag{7}$$

where Af_i is the active firing of the ith hidden node, K is the number of hidden nodes, θ_i is the output value of the ith hidden node, and τ is a small positive constant inserted to ensure that the denominator does not have a value of zero.

When Af_i is larger than the activity threshold Af_o, the hidden node i is an active node. This hidden node will be split into some new nodes in the hidden layer.

The centers and the radiuses of the new splitting hidden nodes can be designated as

$$\boldsymbol{\mu}_{i,j} = \alpha_j\boldsymbol{\mu}_i + \beta_j\mathbf{x}, \quad \sigma_{i,j} = \alpha_j\sigma_i, \quad j=1,2,\ \ldots\ ,N_{\text{new}}, \tag{8}$$

where $0.95<\alpha_j<1.05$ and $0<\beta_j<0.1$, $\boldsymbol{\mu}_i$ and σ_i are the center and radius of the ith hidden node, and N_{new} is the number of the new splitting nodes, which is decided by the rate Af_i.

The weights for the new nodes and the output layer are

$$w_{i,j} = \zeta_j\frac{w_i\cdot\theta_i(t)-e(t)}{N_{\text{new}}\cdot\theta_{i,j}(t)}, \quad \sum_{j=1}^{N_{\text{new}}}\zeta_j = 1, \quad j=1,2,\ \ldots\ ,N_{\text{new}}, \tag{9}$$

where ζ_i is the allocating parameters for the new nodes, $\theta_i(t)$ is the output value of the ith hidden node, $\theta_{i,j}(t)$ is the output value of the new splitting jth hidden node, w_i is the weight of the ith hidden node, $e(t)$ is the current approximation error of the RBFNN

$$e(t) = \hat{y}(t)-y(t), \tag{10}$$

$\hat{y}(t)$ is the output of the neural network and $y(t)$ is the system output for the current input sample $\mathbf{x}$ at time t.

Case 2. Node-Adjusting Mechanism

Free of assumptions about the nature of the underlying joint distribution, the MI provides a natural quantitative measure of the degree of statistical dependence between the stochastic variables (Krivov, Ulanowicz, & Dahiya, 2003). The definition of the MI between two stochastic variables θ_i and Y is

$$M(\theta_i;Y) = \sum_{\theta,y}p(\theta_i,Y)\log_2\frac{p(\theta_i,Y)}{p(\theta_i)p(Y)}, \tag{11}$$

where $p(\theta_i, Y)$ is the joint distribution and $p(\theta_i)$ and $p(Y)$ are the probability density functions. In this paper, θ_i is the output value of the ith hidden node, whereas Y is the network's output (if and only if the two variables θ_i and Y are statistically independent, i.e., $p(\theta_i,Y)=p(\theta_i)p(Y)$).

The magnitude of the MI between two nodes is dependent on the information content of the nodes in terms of their Shannon entropy $H(\theta_i)$ and $H(Y)$. This becomes clear through if one considers the relation (Krivov et al. 2003)

$$M(\theta_i;Y) = H(\theta_i)-H(\theta_i|Y) = H(Y)-H(Y|\theta_i). \tag{12}$$

where $COV(\theta_i)$ is a covariance of θ_i, ε is equal to exp(1), and K is the number of hidden nodes.

The MI is non-negative and equal to zero if and only if the two variables θ_i and Y are statistically independent:

$$M(\theta_i;Y) \le \min(H(\theta_i),H(Y)). \tag{13}$$

This bound, taken together with $M(\theta_i;\ Y)\ge 0$, implies that the normalized MI $m(\theta_i;\ Y)$ is as follows:

$$m(\theta_i;Y) = \frac{M(\theta_i;Y)}{\min(H(\theta_i),H(Y))}, \tag{14}$$

where $0\le m(\theta_i;\ Y)\le 1$. On this basis, more restricted measures of statistical dependence such as cross-correlation have also been used to identify putative links between simultaneously recorded nodes.

In the RBFNN's structure, nodes i and Y in the hidden and the output layer are connected if and only if the normalized MI $m(\theta_i;\ Y)$ is positive (Fig. 3(a)) and if the normalized MI $m(\theta_i;\ Y)$ is equal to zero, which means that nodes θ_i and Y are independent (Fig. 3(b)). The details of the definition can be seen in Fig. 3.

The main steps in the proposed SORBFNN algorithm can be summarized as follows.

Step 1. Create an initial RBFNN consisting of three layers: an input layer, a hidden layer, and an output layer. The number of nodes in the input and output layers is the same as the number of input and output variables in the problem that is being solved. The number of nodes in the hidden layer is randomly generated. All of the parameters should be initialized with the centers, radiuses, and connection weights of the RBFNN uniformly distributed within a small range.

Step 2. For the input sample $\mathbf{x}(t)$, train the RBFNN using training rule

$$\mathbf{W}(t+1) = \mathbf{W}(t)+\dot{\mathbf{W}}(t). \tag{15}$$

Then, the centers and radiuses are adjusted using the gradient method (Qiao & Han, 2010). The mean squared error (MSE) is defined as

$$E = \frac{1}{2T}\sum_{t=1}^{T}e^2(t), \tag{16}$$

T is the number of training samples.

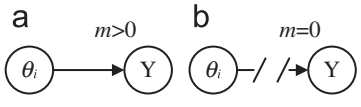

Fig. 3. The correlation between nodes θ_i and Y.

Step 3. Compute the active firing rate of the hidden nodes, *AF*, using Eq. (7). New nodes are inserted according to the activity threshold Af_o. If $Af_i > Af_o$, go to step 4; otherwise, go to step 5.
Step 4. Split the ith hidden node, and insert new hidden nodes. The initial parameters of the new inserted nodes can be obtained from formulas (8,9).
Step 5. If $m(\theta_j; Y)$ is less than the threshold m_0, go to step 6. Otherwise, go to step 7. The threshold m_0 is defined by the designers of the algorithm.
Step 6. Delete the connection between the hidden node j and the output node Y; update the remaining RBFNN parameters. Find the node κ in the hidden layer with the minimal Euclidean distance for node j. The parameters of the hidden node κ are adjusted as follows

$$\begin{aligned}&\boldsymbol{\mu}_{\kappa,\text{after}} = \boldsymbol{\mu}_{\kappa,\text{before}}, \quad \sigma_{\kappa,\text{after}} = \sigma_{\kappa,\text{before}},\\ &w_{\kappa,\text{after}} = w_{\kappa,\text{before}} + w_j \frac{\theta_j(\mathbf{x}(t))}{\theta_{\kappa,\text{before}}(\mathbf{x}(t))},\end{aligned} \tag{17}$$

where $w_{\kappa,\text{before}}$ and $w_{\kappa,\text{after}}$ are the connecting weights of the hidden node κ before and after the structural adjustments, $\boldsymbol{\mu}_{\kappa,\text{before}}$ and $\boldsymbol{\mu}_{\kappa,\text{after}}$ are the center of the hidden node κ before and after node j is deleted, and $\sigma_{\kappa,\text{before}}$ and $\sigma_{\kappa,\text{after}}$ are the radius of the hidden node κ before and after node j is deleted.
Step 7. $t=t+1$, go to Step 2. Stop when $t=T$.

SORBF can insert or prune the hidden nodes depending on the activities of the latter and the connecting MI. This execution behavior indicates that SORBF does not guide the RBFNN design process in a predefined and fixed way. The design scheme used in SORBF is a new and efficient method of RBFNN structure design. The proposed self-organizing algorithm can be used to determine a suitable structure for improving RBFNN performance. This feature is useful for the applications like WWTPs, in which the systems in question are represented by dynamic models.

3. The convergence of SORBF-MPC

For the proposed SORBF-MPC, the convergence of the SORBF with the topology adjustments is an important issue and requires careful investigation, as it is crucial for the successful applications. First, the convergence in the case without structural changes is determined. Then, the convergence in the structural change phase is determined by taking into account both the construction and pruning processes. Furthermore, through this analysis, one obtains a better understanding of the weight-adjusting algorithms.

3.1. Non-changing phase

Convergence in the case without structural changes will be studied in this section. This analysis can be conducted using the convergence theorem.

The nonlinear dynamical systems considered in this paper are modeled using the following differential equation (Yüzgeç et al., 2008)

$$\dot{y}(t) = f(y(t),\mathbf{x}(t)), \quad y(t_0) = y_0, \tag{18}$$

where $y \in \Re$, $\mathbf{x}(t)=[y(t-1), \ldots, y(t-n_y), u(t-1-t_d),\ldots, u(t-n_u-t_d)]^T$. The function $f(\cdot,\cdot)$ is assumed to be unknown. To facilitate the discussion of the convergence, Eq. (18) is then expressed in the following form

$$g(y(t),\mathbf{x}(t)) = \dot{y}(t)+y(t). \tag{19}$$

where $g(\cdot,\cdot)$ is a nonlinear function.

The RBF network with n_y+n_u inputs and one output $\hat{y}$ will be used to approximate the unknown function in real time or, equivalently, the unknown dynamic system (18)). The output of the extended RBFNN can be written as (Han & Qiao, 2012)

$$\hat{g}(y(t),\mathbf{x}(t)) = \mathbf{W}\phi(y(t),\mathbf{x}(t)), \tag{20}$$

where $\phi(y(t),\mathbf{x}(t)) \in \Re^{K\times 1}$, $\hat{g}(\cdot,\cdot)$ is a nonlinear function, and K is the number of hidden nodes.

The extended RBFNN can be rewritten in the following form:

$$\hat{g}(y(t),\mathbf{x}(t)) = \dot{\hat{y}}(t)+\hat{y}(t). \tag{21}$$

Note that the approximation error is defined as in Eq. (10). Combining (18) and (21), one can obtain the approximation error dynamics

$$\begin{aligned}\dot{e}(t) &= \dot{\hat{y}}(t)-\dot{y}(t)\\ &= -\hat{y}(t)+\hat{g}(y(t),\mathbf{x}(t))+y(t)-g(y(t),\mathbf{x}(t))\\ &= -(\hat{y}(t)-y(t))+\hat{g}(y(t),\mathbf{x}(t))-g(y(t),\mathbf{x}(t))\\ &= -e(t)+\hat{g}(y(t),\mathbf{x}(t))-g(y(t),\mathbf{x}(t)).\end{aligned} \tag{22}$$

If there exists a $\mathbf{W}^*$ such that

$$g(y(t),\mathbf{x}(t)) = \mathbf{W}^*\phi(y(t),\mathbf{x}(t)), \tag{23}$$

where each element of $\mathbf{W}^*$ is a constant, the adaptation parameter error is defined as $\Xi = \mathbf{W}-\mathbf{W}^*$.

For $\Xi \in \Re^{1\times K}$, its Frobenius norm satisfies

$$\|\Xi\|_F^2 = \sum_{i=1}^{K}\sum_{j=1}^{1} \vartheta_{ij}^2 = \text{trace}(\Xi\Xi^T), \tag{24}$$

and

$$\frac{\mathrm{d}}{\mathrm{d}t}(\text{trace}(\Xi\Xi^T)) = 2\sum_{i=1}^{K}\sum_{j=1}^{1}\vartheta_{ij}\dot{\vartheta}_{ij} = 2\text{trace}(\Xi\dot{\Xi}^T), \tag{25}$$

where $\dot{\Xi} = \mathrm{d}\Xi/\mathrm{d}t = \dot{\mathbf{W}}$. The weight adaptation strategy is defined as

$$\dot{\mathbf{W}}^{\mathrm{T}} = \eta\phi(y(t),\mathbf{x}(t))e, \tag{26}$$

where $\eta > 0$ is the learning rate for connecting weights.

To prove the convergence of the proposed algorithm, the following Lyapunov function candidate is considered:

$$V = V(e,\Xi) = \tfrac{1}{2}(e^2+\tfrac{1}{n}\text{trace}(\Xi\Xi^T)). \tag{27}$$

The error dynamics Eq. (22) can be represented as

$$\begin{aligned}\dot{e}(t) &= -e(t)+\hat{g}(y(t),\mathbf{x}(t))-g(y(t),\mathbf{x}(t))\\ &= -e(t)+\mathbf{W}\phi(y(t),\mathbf{x}(t))-\mathbf{W}^*\phi(y(t),\mathbf{x}(t))\\ &= -e(t)+(\mathbf{W}-\mathbf{W}^*)\phi(y(t),\mathbf{x}(t))\\ &= -e(t)-\Xi\phi(y(t),\mathbf{x}(t)).\end{aligned} \tag{28}$$

Then, the time derivative of V is

$$\begin{aligned}\dot{V}(e,\Xi) &= e\dot{e}+\tfrac{1}{n}\text{trace}(\Xi\dot{\Xi}^T)\\ &= e(-e-\Xi\phi(y(t),\mathbf{x}(t)))+\tfrac{1}{n}\text{trace}(\Xi\dot{\mathbf{W}}^{\mathrm{T}})\\ &= -e^2-e\Xi\phi(y(t),\mathbf{x}(t))+\tfrac{1}{n}\text{trace}(\Xi\dot{\mathbf{W}}^{\mathrm{T}}).\end{aligned} \tag{29}$$

Using the definition and the property of the trace operator,

$$e\Xi\phi(y(t),\mathbf{x}(t)) = \text{trace}(\Xi\phi(y(t),\mathbf{x}(t))e). \tag{30}$$

Using the weight adaptation strategy as in Eq. (26), Eq. (29) will be

$$\begin{aligned}\dot{V}(e,\Xi) &= -e^2-\text{trace}(\Xi\phi(y(t),\mathbf{x}(t))e)+\tfrac{1}{n}\text{trace}(\Xi\dot{\mathbf{W}}^{\mathrm{T}})\\ &= -e^2-\tfrac{1}{n}\text{trace}(\Xi(\eta\phi(y(t),\mathbf{x}(t))e-\dot{\mathbf{W}}^{\mathrm{T}}))\\ &= -e^2-\tfrac{1}{n}\text{trace}(\Xi(\eta\phi(y(t),\mathbf{x}(t))e-\Xi(\eta\phi(y(t),\mathbf{x}(t))e))\\ &= -e^2.\end{aligned} \tag{31}$$

Thus, $\dot{V}$ is negative semidefinite in the (e, Ξ)– space, so $e(t)$ and $\Xi(t)$ are bounded for $t \geq t_0$. Hence, based on the Lyapunov-like lemma

$$\lim_{t\to\infty} e(t) \to 0, \tag{32}$$

the convergence result for the structural non-changing phase has been validated.

Remark: The theorem is stated for the RBFNN with a fixed structure. However, the theorem will also be further studied for the RBFNN with a varying structure, in which the hidden nodes change with time. It is also noteworthy that the structural change may disrupt the convergence of the RBFNN unless the structure design method is suitable.

3.2. Structural change phase

This phase consists of both the node-splitting mechanism described in step 4 and the node-adjusting mechanism described in step 6. It is suggested in this paper that the changes made to the structure influence the current error $e(t)$ for the input sample $\mathbf{x}(t)$ at time t; at time t, there are K hidden nodes in the hidden layer. The convergence of each component is described below.

(1) The node-splitting mechanism in step 4

When the activity node (i.e., the ith node) has been divided into N_{new} new hidden nodes, there are $K+N_{\text{new}}$-1 hidden nodes. The current error $e(t)$ at time t will be given by

$$\begin{aligned} e_{K+N_{\text{new}}-1}(t) &= \hat{y}(t) - y(t) \\ &= \sum_{k=1}^{K+N_{\text{new}}-1} w_k\theta_k(\mathbf{x}(t)) - y(t) \\ &= \left[\sum_{k=1}^{K} w_k\theta_k(\mathbf{x}(t)) - w_i\theta_i(\mathbf{x}(t)) + \sum_{j=1}^{N_{\text{new}}} w_{i,j}\theta_j(\mathbf{x}(t))\right] - y(t), \end{aligned} \tag{33}$$

where $\hat{y}(t)$ is the output of the neural network for the current input sample $\mathbf{x}(t)$ and where $y(t)$ is the system output at time t. According to formulas (8,9), the following will be true

$$\sum_{j=1}^{N_{\text{new}}} w_{i,j}\theta_j(\mathbf{x}(t)) - w_i\theta_i(\mathbf{x}(t)) = 0. \tag{34}$$

Eq. (33) can be rewritten as

$$\begin{aligned} e_{K+N_{\text{new}}-1}(t) &= \left[\sum_{k=1}^{K} w_k\theta_k(\mathbf{x}(t)) - w_i\theta_i(\mathbf{x}(t)) + \sum_{j=1}^{N_{\text{new}}} w_{i,j}\theta_j(\mathbf{x}(t))\right] - y(t) \\ &= \sum_{k=1}^{K} w_k\theta_k(\mathbf{x}(t)) - y(t) - e_K(t) \\ &= e_K(t) - e_K(t) = 0. \end{aligned} \tag{35}$$

The error $e(t)$ will change to zero for the current input sample $\mathbf{x}$ at time t. In this structure-changing step, the output MSE for the RBFNN will converge rapidly for the learning process.

(2) The node-adjusting mechanism from step 6

Even when the connection between the hidden node j and the output node Y is cut, the node κ in the hidden layer with the minimal Euclidean distance from node j, the error $e(t)$ will be adjusted using Eq. (17).

$$\begin{aligned} e_{K-1}(t) &= \sum_{k=1,k\neq\kappa}^{K} w_k\theta_k(\mathbf{x}(t)) - y(t) - w_j\theta_j(\mathbf{x}(t)) \\ &\quad + w_{\kappa,\text{after}}\theta_{\kappa,\text{before}}(\mathbf{x}(t)) \\ &= \sum_{k=1,k\neq\kappa}^{K} w_k\theta_k(\mathbf{x}(t)) - y(t) - w_j\theta_j(\mathbf{x}(t)) \\ &\quad + (w_{\kappa,\text{before}} + w_j\frac{\theta_j(\mathbf{x}(t))}{\theta_{\kappa,\text{before}}(\mathbf{x}(t))})\theta_{\kappa,\text{before}}(\mathbf{x}(t)) \\ &= \sum_{k=1,k\neq\kappa}^{K} w_k\theta_k(\mathbf{x}(t)) - y(t) - w_j\theta_j(\mathbf{x}(t)) \\ &\quad + w_{\kappa,\text{before}}\theta_{\kappa,\text{before}}(\mathbf{x}(t)) + w_j\theta_j(\mathbf{x}(t)) \\ &= \sum_{k=1}^{K} w_k\theta_k(\mathbf{x}(t)) - y(t) \\ &= e_K(t). \end{aligned} \tag{36}$$

Consequently, it emerges that the structure-adjusting mechanism will not influence the error $e(t)$ at time t. The output MSE for the RBFNN will not change significantly in the following phases.

This technique creates the following advantages:

1. Each time new nodes are inserted, the network has good convergence. This property guarantees the convergence of the algorithm.
2. Each time the connecting links are cut, the convergence of the proposed algorithm will not be influenced.

As seen in the three phases presented above, the convergence of the proposed SORBF can be maintained or sped up. The learning law proposed in this paper can guarantee the convergence of the SORBF-MPC, which is one of the most important characteristics.

4. Simulation studies

4.1. A plant layout and process model

The WWTP is a dynamic system that involves various physical and biological phenomena as well as large disturbances. Many control strategies intended for use with wastewater treatment plants have been presented in the literature, but it is difficult to evaluate and compare the possible strategies. The results partly from the variability of the influent, the complexity of the physical and biochemical phenomena involved and the large range of time constants inherent in the activated sludge process. A benchmark (i.e., a simulation environment that represents the layout of a particular plant and a simulation system that includes influent loads, test procedures, and evaluation criteria) has been proposed within the framework of COST Actions 682 and 624-BSM1 (Jeppsson & Pons, 2004). In the BSM1, the plant is described as in Fig. 4; it is to be composed of two anoxic units, three aerobic units, and a secondary settler. Each of the units of the bioreactor is assumed to have a constant volume (1000 m^3, 1000 m^3, 1333 m^3, 1333 m^3, and 1333 m^3, respectively) and to be ideally mixed. The secondary settler is assumed to have a constant volume (6000 m^3). The system for each bioreactor unit is established according to the International Association on Water Quality Activated Sludge Model 1 (IAWQ-ASM1) (Henze, Grady, Gujer, Marais, & Matsuo, 1986).

The complete benchmark model is summarized by the following equations.

For $l=1$ (unit 1)

$$\frac{d\mathbf{Z}_1}{dt} = \frac{1}{V_1}(Q_a\mathbf{Z}_5 + Q_r\mathbf{Z}_r + Q_o\mathbf{Z}_o + r_1V_1 - Q_1\mathbf{Z}_1), \tag{37}$$

where $Q_1 = Q_a + Q_r + Q_o$, Q_a is the internal recycle flow rate; Q_r is the external recycle flow rate; Q_o is the influent flow rate; $\mathbf{Z}_1$, $\mathbf{Z}_5$, $\mathbf{Z}_r$, and $\mathbf{Z}_o$ are the component concentrations of unit 1, unit 5, external recycling, and the initial concentration of influent,

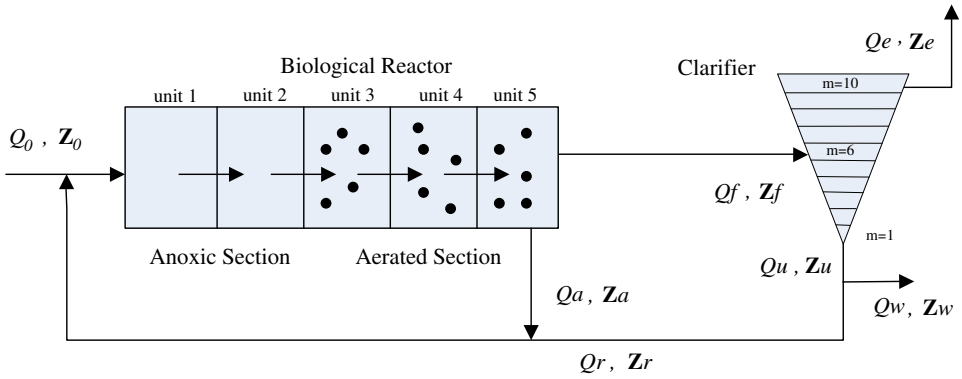

Fig. 4. General overview of the BSM1 plant.

respectively; V_1 is the volume of unit 1; and r_1 is the component reaction rate in unit 1. $\mathbf{Z}$ is expressed as $\mathbf{Z}=[S_S, X_S, X_{B,H}, X_{B,A}, X_P, S_O, S_{NO}, S_{NH}, S_{ND}, X_{ND}]$ as defined in (Jeppsson & Pons, 2004).

For $l=2$–5 (units 2–5)

$$\frac{d\mathbf{Z}_l}{dt}=\frac{1}{V_l}(Q_{l-1}\mathbf{Z}_l+r_lV_l-Q_l\mathbf{Z}_l), \tag{38}$$

where $Q_l=Q_{l-1}$, $\mathbf{Z}_l$ is the component concentration of the lth unit and V_l is the volume of the lth unit.

It is complicated to describe how oxygen is transferred from the air bubbles to the cells of the microorganisms in the overall process. However, the process can be divided into several sub-processes: convective mass transfer within the air bubble to the gas–liquid interface, transportation through the phase border, and mass transfer within the liquid phase to the microbial flocs. The case of oxygen is represented as follows

$$\frac{dS_{O,l}}{dt}=\frac{Q_{l-1}S_{O,l-1}-Q_lS_{O,l}}{V_l}+(K_La)_l(S_{O,\mathrm{sat}}-S_{O,l})+r_l, \tag{39}$$

where V_l is the volume of the lth unit, $S_{O,l-1}$ is the concentration of DO in the l-1th unit (entering the lth unit), $S_{O,l}$ is the concentration of DO in the lth unit, Q_{l-1} is the flow rate of the l-1th unit, Q_l is the flow rate of the lth unit, $(K_La)_l$ is the overall mass transfer coefficient in the lth unit, $S_{O,\mathrm{sat}}$ is the DO saturation concentration and r_l is the rate of use of DO by biomass in the lth unit.

4.2. Influent load and evaluation criteria

(1) Influent load

To derive an objective view of the performance of the control strategy in different situations, simulated influent data from three two-week files derived from real operating data can be used (Jeppsson & Pons, 2004). These files are generated to simulate three different weather situations. The data used for the estimation and control are sampled with a sampling period of 0.25 h (= 15 min) in this paper.

As a multivariable input–output system, the control system is described as follows.

Bounds: The limits on the effluents – ammonium (NH) concentration, total nitrogen (N_{tot}) concentration, suspended solid (SS) concentration, biological oxygen demand over a 5-day period (BOD_5), and COD – are given in Table 2.

Inputs: The two manipulated variables are the internal recycle flow rate Q_a and the mass transfer coefficients in the fifth aerated tanks K_La. The bounds for the input variables are same as in Shen et al. (2009) – $Q_a<96{,}000$ m^3/day and $K_La<360$ day^{-1}. The mass transfer coefficient corresponds to the efficiency of the aeration in a given aerated tank.

Table 2
Bounds for the effluent qualities.

Effluents Qualities	Upper bound
NH (mg/l)	4
N_{tot} (mg/l)	18
SS (mg/l)	30
BOD_5 (mg/l)	10
COD (mg/l)	100

Outputs: The control variable is the DO concentration in the last unit of the bioreactor. Five effluent variables – the ammonium concentration, the concentration of suspended solids, the BOD_5, the COD, and the total nitrogen – are used to demonstrate the performance of the control system.

Disturbances: The measurable disturbances have been considered: the influent flow rate q_o and the influent ammonium concentration NH_o (see Fig. 5) (Shen et al., 2009). The variations of the disturbances around a mean value are considerable and essentially periodical given a 14-day period.

(2) Evaluation criteria

Various criteria have been determined to be useful in assessing the performance of the plant. In this study, AE consumption was used to evaluate control strategies. AE was calculated for the last 7 days of dynamic data. AE consumption is described as in (Jeppsson & Pons, 2004):

$$AE=\frac{24}{7}\int_{t=7}^{t=14}\sum_{l=3}^{5}\left[0.0007\times(K_La)_l(t)^2\left(\frac{V_l}{1333}\right)+0.3267\times(K_La)_l(t)\left(\frac{V_l}{1333}\right)\right]dt, \tag{40}$$

where $(K_La)_l$ is the overall mass transfer coefficient in the lth unit and V_l is the volume of the lth unit. In this case, a rough estimate of average electricity price in the EU (0.1 €/kW h) was taken into account, and thus, all of the weights were multiplied by 0.1.

4.3. SORBF modeling and evaluation

In this paper, the SORBF-MPC strategy is proposed as a means of controlling the DO concentration based on the BSM1. It is intended to control the DO level in the final compartment of the reactor (Unit 5) by manipulating the oxygen transfer coefficient K_La and the internal flow recirculation Q_a.

For MISO processes, a MISO SORBF model has been developed. The parameters to be determined for each MISO model are the model input and output orders n_y and n_u, the delay time t_d, and the number of hidden layer nodes K. A previous study focused on

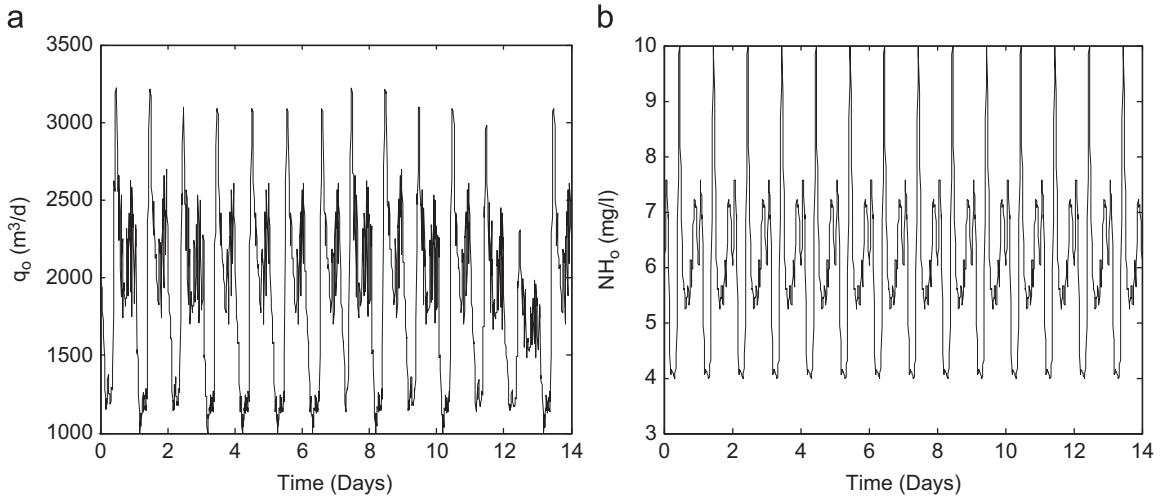

Fig. 5. Disturbances of influent flow rates and influent ammonium concentration. (a) Disturbance of influent flow rates and (b) Disturbance of influent ammonium concentration.

determining the model input and output order for the activated sludge process was given in (Stare, Vrecko, Hvala, & Strmcnik, 2007). In addition, the recommended time delay $t_d=4$ is directly used. Finally, the SORBF model chosen in this research is

$$\hat{y}(t)=f(y(t-1),y(t-2),Q_a(t-5),Q_a(t-6),K_La(t-5),K_La(t-6)), \quad (41)$$

where $y(t)$ and $\hat{y}(t)$ denote the process output and the network output; K_La is the oxygen transfer coefficient and Q_a is the internal flow recirculation.

The effectiveness of the SORBF model is evaluated via on-line modeling and multistep-ahead prediction. The prediction is compared with a pretrained fixed structure multi-layer perceptron (MLP) model (Chandramouli, Brion, Neelakantan, & Lingireddy, 2007) and the two self-organizing RBF models – the minimal resources-allocating network (MRAN) (Panchapakesan, Palaniswami, Ralph, & Manzie, 2002) and the growing and pruning algorithm for RBF (GGAP-RBF) (Bortman & Aladjem, 2009) model. In the simulation, the neural network Eq. (41) model is used. First, 15 hidden nodes are used for MLP, and 10 initial hidden nodes are used for the proposed SORBF, MRAN, and GGAP-RBF. In the training period, the SORBF can both adjust the weights and change the network structure. Then, the suitable network models for the current operating point are selected and used for five step-ahead predictions. In the simulations, the fixed-parameter model for the DO concentration has 15 hidden nodes that are chosen to match the average number of hidden nodes in the adaptive network to ensure a fair comparison. The hidden nodes of the proposed SORBF for the DO concentration are displayed in Fig. 6.

Five step-ahead predictions by the adaptive models (with disturbances) are displayed together with the real process output in Fig. 7 for comparison. To determine the modeling abilities of the different methods, the set points of DO concentration are tuned dramatically. The real DO concentration values derive from the BSM1 in the open-loop simulation.

Clearly, the predictions obtained using the proposed SORBF model with respect to the real output is more accurate than those obtained from the other models. Performance is assessed using the number of hidden nodes and the MSE as in Eq. (16). The details are presented in Table 3. Table 3 shows the different models used for the three types of weather: dry, rainy, and stormy. The structures of MRAN, GGAP-RBF, and the proposed SORBF model are self-adaptive. The final structure of the proposed SORBF model is the most compact. In additon, the MSE of the SORBF model is the smallest. The comparisons demonstrate that the SORBF model is suitable for wastewater treatment modeling.

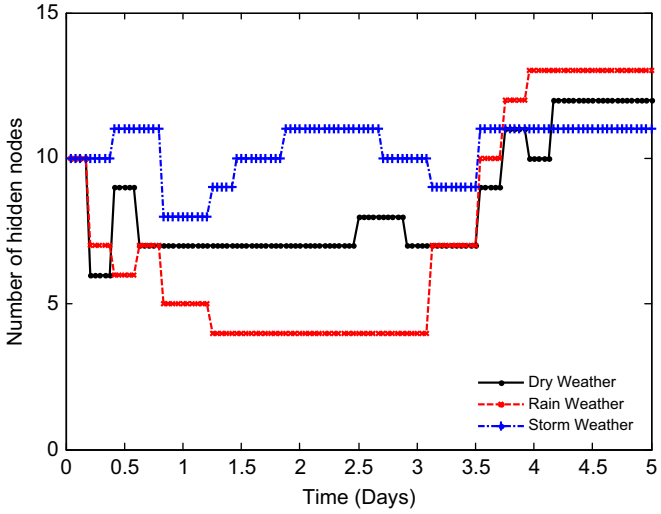

Fig. 6. Hidden nodes adjusting in the SORBF model for DO concentration.

4.4. On-line MPC control

The use of the SORBF model in MPC for wastewater treatment systems has been studied in this paper. The SORBF-MPC strategy is shown in Fig. 1. In this approach, a SORBF neural network model predicts the future process response over the specified horizon. The predictions are used in a numerical optimization routine that attempts to minimize a specified cost function (1) in searching for an optimal control signal u at each sample instant.

Prior to on-line control, simulations have been performed to obtain a set of suitable control parameters. The parameters of the prediction and control horizon, the weights and the set point trajectory of the MPC affect the closed-loop behavior of the plant. The weights in the cost function may be set based on the economic objectives of the plant, but they are usually adjusted in such a way that satisfactory control performance is achieved. In this case, the parameters are tuned based on experience gained from the simulations and based on the tuning rules presented in

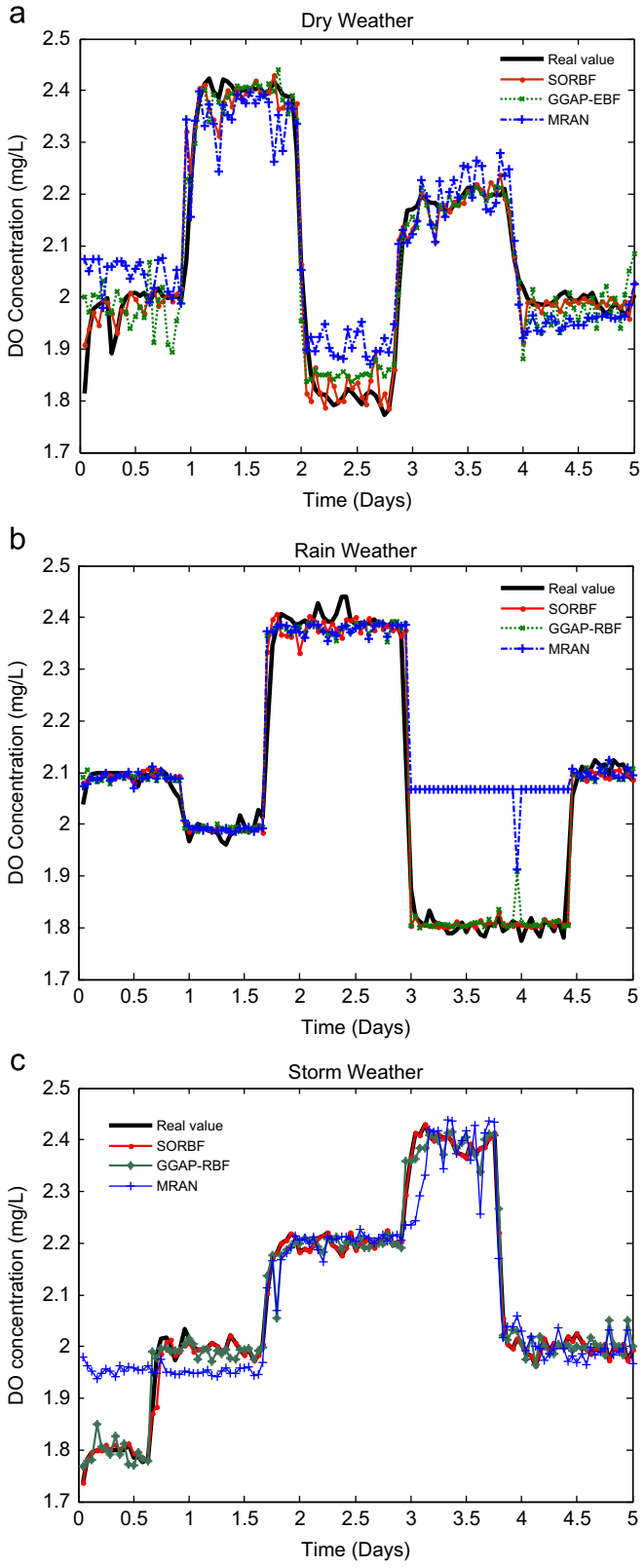

Fig. 7. Five step-ahead prediction of DO concentration using the models.

(Stare et al., 2007). The parameters of the MPC can be summarized as follows:

$$W_i^y = [1], \quad W_j^u = \begin{bmatrix} 1 & 0 \\ 0 & 1 \end{bmatrix}, \quad H_p = 5, \quad H_u = 1. \tag{42}$$

Table 3
A comparison of the performance of different models (all results were averaged based on 20 independent runs).

Weather	Models	Hidden nodes	MSE (5-step)
Dry	**SORBF**	**12 ± 1**	**0.0130**
	MLP	15	0.0386
	MRAN	17 ± 5	0.0250
	GGAP-RBF	12 ± 1	0.0206
Rain	**SORBF**	**13 ± 1**	**0.0132**
	MLP	15	0.0901
	MRAN	18 ± 4	0.0411
	GGAP-RBF	14 ± 1	0.0398
Storm	**SORBF**	**11 ± 1**	**0.0127**
	MLP	15	0.0623
	MRAN	17 ± 4	0.0287
	GGAP-RBF	12 ± 1	0.0193

Quadratic programming is used to minimize Eq. (1) due to the quadratic form of the objective function. The control variables are bounded as shown in Eq. (2), and therefore, constrained optimization is used. Moreover, because the control variables are nonlinearly relevant to the model output in the RBF model, the sequential quadratic programming algorithm is used in the MPC scheme. The RBF model adaptation and the MPC algorithm are implemented using Matlab for the simulation and on-line control. The initial values of the control variables to be optimized are set using the actual values from the last sample.

For the sake of comparison, three other controllers have been designed for the treatment process: the proportional–integral (PI) controller (Ayesa et al., 2006), MPC (Holenda et al., 2008) and multivariable PID (MPID) controller (Wahaba et al., 2009). To ensure a fair comparison, the optimal parameters of the controllers are the same as in the initial papers. The equation for the integrated absolute error (IAE) is defined as

$$IAE(t) = \frac{1}{T}\sum_{t=1}^{T} |y(t) - y_d(t)|, \tag{43}$$

where $y(t)$ and $y_d(t)$ are the output and desired output of the system, respectively, and T is the total number of samples.

In this simulation, the alternating sludge process is realized by changing the DO set point between 1.5 and 2.5 mg/l in the bioreactor (Holenda et al., 2008; Shen et al., 2009). The manipulated variable (oxygen mass transfer coefficient K_La) varies from 0 to 360 day^{-1} to reach the desired DO level using the proposed SORBF-MPC (O'Brien et al., 2011).

The on-line control results (dry weather) are displayed in Figs. 8–10, including the real process responses and the control variables used to track step changes in the set points with the above MPC settings via the proposed SORBF-based MPC method. The graphs in Fig. 8 show that the SORBF-MPC model can track the set points of the DO concentrations in the dry weather case. The errors indicating the difference between the set-point values and the control output remain within the range of ±0.1 mg/l (±5%). The two manipulated variables are shown in Figs. 9 and 10. The graphs in Figs. 8–10 indicate that the suitable control signals Q_a and K_La drive the process response, following the set points, and that the input variables do not exceed the upper bound. The basic control strategy in benchmark simulation study (Jeppsson & Pons, 2004) is used as a reference case for comparison purposes. The AE consumption used is AE = 724 €/d in the open loop control condition as in O'Brien et al. (2011) and Stare et al. (2007). The details of the comparisons in the dry weather case are shown in Tables 4–5.

As Table 4 indicates, a lower AE value is achieved with the SORBF-MPC model (8.6%). The best DO concentration tracking

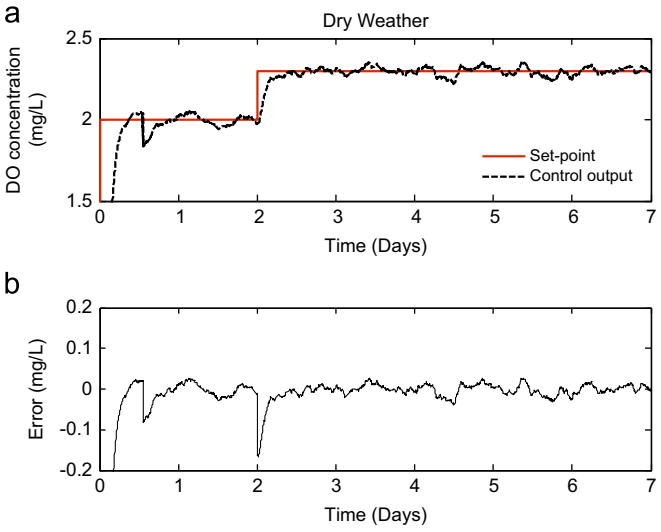

Fig. 8. On-line tracking control performance in the dry weather case.

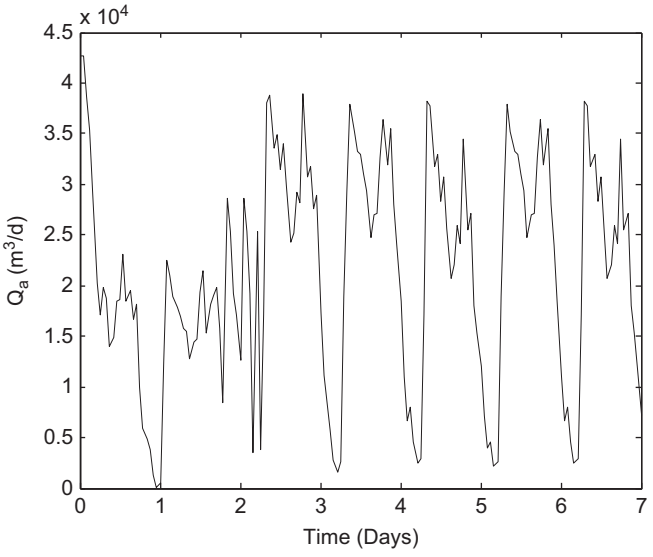

Fig. 9. On-line Q_a performance in the dry weather case.

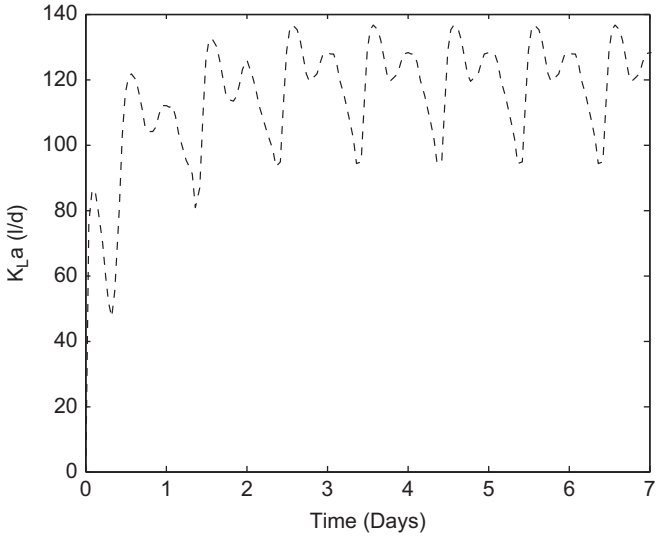

Fig. 10. On-line K_La of the 5th unit in the dry weather case.

Table 4
A comparison of the IAE and AE of different controllers in dry weather case (five step-ahead predictions).

Weather	Controllers	IAE (mg/l)	AE (€/d)
Dry	**SORBF-MPC**	**0.052 (2.6%)**	**662 (−8.6%)**
	PI	0.218 (10.9%)*	678 (−6.4%)*
	MPC	0.089 (4.45%)*	677 (−6.5%)*
	MPID	0.134 (6.7%)*	637 (−12.1%)*

Table 5
A comparison of the effluent qualities with different controllers in dry weather case (five step-ahead predictions).

	Mean Effluent Qualities				
	NH (mg/l)	N_{tot} (mg/l)	SS (mg/l)	BOD_5 (mg/l)	COD (mg/l)
Limit	4	18	30	10	100
SORBF-MPC	**1.98**	**14.64**	**14.35**	**2.61**	**41.41**
PI	3.03*	16.49*	13.55	3.71	54.80
MPC	1.78*	15.87*	14.17*	2.87*	49.66*
MPID	2.26*	14.53*	14.53	2.93	50.00

* The results are listed in the original papers.

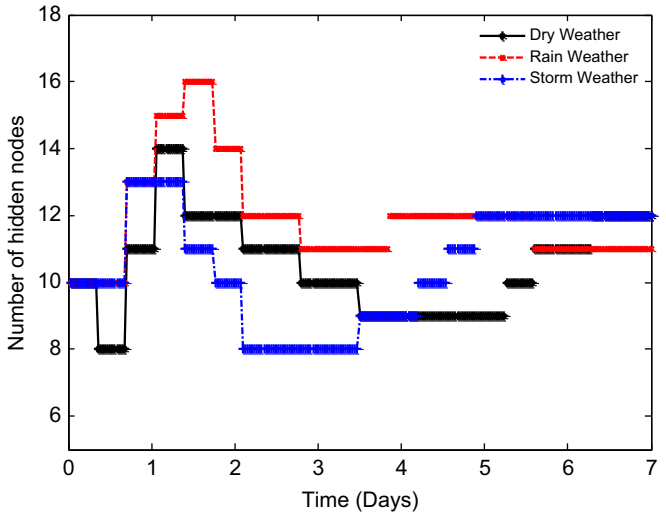

Fig. 11. Hidden nodes variation in the adaptive model.

control is achieved when SORBF-MPC is employed in the dry weather case. Meanwhile, Table 5 illustrates the average effluent qualities according to the proposed SORBF-MPC – 1.98 mg/l, 14.64 mg/l, 14.35 mg/l, 2.61 mg/l, and 41.41 mg/l, respectively, for the concentration of NH, N_{tot}, SS, BOD_5, and COD. These results show that the qualities of the effluent can be controlled well using the SORBF-MPC model and can thereby comply with regulations. The best BOD_5 and COD removal is achieved by SORBF-MPC. SORBF-MPC also yields better NH concentration than the PI and MPID models, better N_{tot} concentration than PI and MPC, and better SS concentration than MPID.

The hidden nodes of the SORBF shown in Fig. 11 are adjusted in the modeling. The graphs in Fig. 11 show that the variation in the hidden nodes is drastic in the adaptive model at the beginning. This is because the test data are different from the pretraining data and the model needs more centers to satisfy the MSE criterion. The details of the comparisons in the rain weather case and the storm weather case are given in Table 6, which proves that the proposed SORBF-MPC model is sufficient

Table 6
Comparisons of the performance of different controllers in both the rain weather and storm weather cases (five step-ahead predictions).

Weather	Controllers	IAE (mg/l)	AE (€/kW h)
Rain	**SORBF-MPC**	**0.081 (4.5%)**	**663 (−8.4%)**
	PI	0.256 (12.8%)*	698 (−3.6%)
	MPC	0.150 (7.5%)*	691 (−4.6%)
	MPID	0.166 (8.3%)*	653 (−9.8%)*
Storm	**SORBF-MPC**	**0.064 (3.2%)**	**663 (−8.4%)**
	PI	0.231 (11.5%)*	692 (−4.4%)
	MPC	0.105 (5.25%)	687 (−5.1%)
	MPID	0.142 (7.1%)	648 (−10.5%)*

* The results are listed in the original papers.

Table 7
Performance of the proposed SORBF-MPC controller with different prediction horizons.

Prediction horizon	$H_p=1$	$H_p=3$	$\boldsymbol{H_p=5}$	$H_p=10$
Dry weather				
Set point (mg/l)	2.0-2.4	2.0-2.4	**2.0-2.4**	2.0-2.4
IAE (mg/l)	0.051	0.051	**0.052**	0.214
Max deviation ΔK_La	43.37	30.12	**23.47**	19.33
Rain weather				
Set point (mg/l)	1.8-2.3	1.8-2.3	**1.8-2.3**	1.8-2.3
IAE (mg/l)	0.78	0.080	**0.081**	0.432
Max deviation ΔK_La	41.36	31.34	**24.91**	21.67
Storm weather				
Set point (mg/l)	1.8-2.3	1.8-2.3	**1.8-2.3**	1.8-2.3
IAE (mg/l)	0.57	0.062	**0.064**	0.312
Max deviation ΔK_La	43.51	30.46	**24.57**	19.97

for good performance in both cases. It is noted that the SORBF-MPC model displays better robustness in this simulation. This is because measurable disturbances (both the influent flow rate q_o and the influent ammonium concentration NH_o) have been considered in the process.

Simulations were performed using several parameter settings to evaluate the performance of the controller during the 7-day observation period. The chosen DO set points for the bioreactor ranged from 1.5 to 2.5 mg/l (Holenda et al., 2008; Shen et al., 2009). The results obtained using the SORBF-MPC controller with different prediction horizons are shown in Table 7. Clearly, when the prediction horizon is $H_p=5$, the IAE value is acceptable, and the increase overshoot of the max deviation ΔK_La is smooth.

4.5. Analysis of the simulation results

MPC is widely used in many industrial applications, and the above results have proved it to be an efficient method of controlling the wastewater treatment process. For comparison purposes, the PI (Ayesa et al., 2006), MPC (Holenda et al., 2008), and multivariable PID (MPID) (Wahaba et al., 2009) methods are also employed for the same system to illustrate their performance. Tables 4–6 show that the SORBF-MPC and MPC methods yield smaller IAE values than do the PI and MPID controllers in the three weather cases. According to the results of the paper, the proposed SORBF-MPC controller can be effectively used to control the DO concentration of wastewater treatment plants.

To gain a deeper understanding of the proposed SORBF-MPC, the control performances of the two controllers – SORBF-MPC and the MPC (Holenda et al., 2008) – were analyzed. Because the control schemes used by the two methods are the same, this control strategy focused on modeling methods. In the MPC method (Holenda et al., 2008), the aeration processes are designed through continuous spate–space matrices. In contrast, the proposed SORBF-MPC method is established based on the SORBF, which can change the structure of the RBFNN to make it consistent with the nonlinear characteristics of the process (see Fig. 11). Therefore, it is not surprising that the control performance of the SORBF-MPC model is better than that of the MPC model (see Tables 4–6).

Moreover, the results associated with different prediction horizons can affect the IAE value of the controller. When the prediction horizon is small, the IAE values of the control results will decrease (see Table 7). However, the lower prediction horizon will increase overshot and cause rapid changes in the manipulated variable, which can be avoided by imposing constraints on the manipulated variable. This conclusion is the same as that in Holenda et al. (2008).

5. Conclusion

This paper has introduced a variable structure RBF for addressing the MPC of the DO concentration in wastewater treatment system. This approach is different from traditional MPC approaches because its learning algorithm actually addresses the characteristics of the system. The major advantage of the SORBF predictive controller is that updates based on the weight and the hidden nodes of the RBF keep the model attuned with the current system dynamics. The hidden nodes are selected on-line based on the node activity and the MI, which greatly improves the model accuracy, whereas the weights of the RBF are not adjusted. This method enhances the capacity of the RBF model to adapt to nonlinear dynamic systems. The adaptive model developed in this research is shown to yield more accurate predictions than the fixed models and the other self-adaptive models in the WWTP context.

The on-line control performance shows that the control-oriented adaptive RBF network can model nonlinear system dynamics and therefore performs well in the entire operating space although the plant dynamics are operating point dependent. It is observed that the SORBF-MPC model can control the DO concentration effectively. The model changes are effective in capturing the plant dynamics, and such adaptive model-based control significantly improves control performance.

The extensive simulations reported on this paper have been conducted to comparatively evaluate how well SORBF-MPC performed with regard to the DO concentration, AE and effluent qualities. In the future, an improved SORBF-MPC might control the nitrate concentration in the second anoxic tank. In addition, for a MPC scheme, the prediction horizon and the control horizon are small in this paper. A new SORBF-MPC control strategy with a large prediction horizon and control horizon for optimizing operating costs within the activated sludge process will be discussed in the future. The additional control strategy will save energy with a time-varying DO set point based on the influent and effluent water concentration.

Acknowledgment

The authors would like to thank Prof. Wen Yu for reading the manuscript and providing valuable comments. The authors also would like to thank the anonymous reviewers for their valuable comments and suggestions, which helped improve this paper greatly.

References

Ayesa, E., Sota, A. D., Grau, P., Sagarna, J. M., Salterain, A., & Suescun, J. (2006). Supervisory control strategies for the new WWTP of Galindo–Bilbao: the long run from the conceptual design to the full-scale experimental validation. *Water Science and Technology*, *53*(4-5), 193–201.

Azwar, Rashid, M. M., & Hussain, M. A. (2008). Design of AI neural network based controller for controlling dissolved oxygen concentration in a sequencing batch reactor. *International Journal of Knowledge-based and Intelligent Engineering Systems*, *12*(2), 121–136.

Bortman, M., & Aladjem, M. (2009). A growing and pruning method for radial basis function networks. *IEEE Transactions on Neural Networks*, *20*(6), 1039–1045.

Carlsson, B., & Rehnstrom, A. (2002). Control of an activated sludge process with nitrogen removal—a benchmark study. *Water Science and Technology*, *45*(4-5), 135–142.

Carlsson, B., Lindberg, C. F., Hasselblad, S., & Xu, S. (1994). On-line estimation of the respiration rate and the oxygen transfer rate at Kungsangen wastewater plant in Uppsala. *Water Science and Technology*, *30*(4), 255–263.

Chachuat, B., Roche, N., & Latifi, M. A. (2005). Optimal aeration control of industrial alternating activated sludge pants. *Biochemical Engineering Journal*, *23*(3), 277–289.

Chandramouli, V., Brion, G., Neelakantan, T. R., & Lingireddy, S. (2007). Backfilling missing microbial concentrations in a riverine database using artificial neural networks. *Water Research*, *41*(1), 217–227.

Ferrer, J., Rodrigo, M. A., Seco, A., & Penyaroja, J. M. (1998). Energy saving in the aeration process by fuzzy logic control. *Water Science and Technology*, *38*(3), 209–217.

Han, H. G., & Qiao, J. F. (2012). An adaptive computation algorithm for RBF neural network. *IEEE Transactions on Neural Networks and Learning Systems*, *23*(2), 1–6.

Henze, M., Grady, C.. P. L.., Gujer, W., Marais, G.R., & Matsuo, T. (1986). Activated sludge model no. 1. IAWQ Scientific and Technical Report no. 1, London, UK.

Holenda, B., Domokos, E., Redey, A., & Fazakas, J. (2007). Aeration optimization of a wastewater treatment plant using genetic algorithm. *Optimal Control Applications and Methods*, *28*(3), 191–208.

Holenda, B., Domokos, E., Redey, A., & Fazakas, J. (2008). Dissolved oxygen control of the activated sludge wastewater treatment process using model predictive control. *Computers and Chemical Engineering*, *32*(6), 1270–1278.

Huang, M. Z., Wan, J. Q., Ma, Y. W., Wang, Y., Li, W. J., & Sun, X. F. (2009). Control rules of aeration in a submerged biofilm wastewater treatment process using fuzzy neural networks. *Expert Systems with Applications*, *36*(7), 10428–10437.

Jeppsson, U., & Pons, M. N. (2004). The COST benchmark simulation model—current state and future perspective. *Control Engineering Practice*, *12*(4), 299–304.

Krivov, S., Ulanowicz, R. E., & Dahiya, A. (2003). Quantitative measures of organization for multiagent systems. *Biosystems*, *69*(1), 39–54.

Kruszewski, A., Wang, R., & Guerra, T. M. (2008). Nonquadratic stabilization conditions for a class of uncertain nonlinear discrete time TS fuzzy models: a new approach. *IEEE Transactions on Automatic Control*, *53*(2), 606–611.

Lee, H., Lee, K. M., Park, C. H., & Park, Y. H. (2005). Application of remote monitoring and automatic control system using neural network for small wastewater treatment plants in Korea. *Water Science and Technology*, *51*(10), 249–257.

O'Brien, M., Mack, J., Lennox, B., Lovett, D., & Wall, A. (2011). Model predictive control of an activated sludge process: a case study. *Control Engineering Practice*, *19*(1), 54–61.

Panchapakesan, C., Palaniswami, M., Ralph, D., & Manzie, C. (2002). Effects of moving the centers in an RBF network. *IEEE Transactions on Neural Networks*, *13*(6), 1299–1307.

Qiao, J. F., & Han, H. G. (2010). A repair algorithm for RBF neural network and its application to chemical oxygen demand modeling. *International Journal of Neural Systems*, *20*(1), 63–74.

Shannon, M. A., Bohn, P. W., Elimelech, M., Georgiadis, J. G., Marinas, B. J., & Mayes, A. M. (2008). Science and technology for water purification in the coming decades. *Nature*, *452*, 301–310.

Shen, W., Chen, X., Pons, M. N., & Corriou, J. P. (2009). Model predictive control for wastewater treatment process with feedforward compensation. *Chemical Engineering Journal*, *155*(1-2), 161–174.

Shen, W. H., Chen, X. Q., & Corriou, J. P. (2008). Application of model predictive control to the BSM1 benchmark of wastewater treatment process. *Computers and Chemical Engineering*, *32*(12), 2849–2856.

Stare, A., Vrecko, D., Hvala, N., & Strmcnik, S. (2007). Comparison of control strategies for nitrogen removal in an activated sludge process in terms of operating costs: a simulation study. *Water Research*, *41*(9), 2004–2014.

Syu, M. J., & Chen, B. C. (1998). Back-propagation neural network adaptive control of a continuous wastewater treatment process. *Industrial Engineering Chemistry Research*, *37*(9), 3625–3630.

Traore, A., Grieu, S., Puig, S., Corominas, L., Thiery, F., Polit, M., & Colprim, J. (2005). Fuzzy control of dissolved oxygen in a sequencing batch reactor pilot plant. *Chemical Engineering Journal*, *111*(1), 13–19.

Wahaba, N. A., Katebia, R., & Balderud, J. (2009). Multivariable PID control design for activated sludge process with nitrification and denitrification. *Biochemical Engineering Journal*, *45*(3), 239–248.

Wu, X. J., Zhu, X. J., Cao, G. Y., & Tu, H. Y. (2008). Predictive control of SOFC based on a GA-RBF neural network model. *Journal of Power Sources*, *179*(1), 232–239.

Yüzgeç, U., Becerikli, Y., & Türker, M. (2008). Dynamic neural-network-based model-predictive control of an industrial baker's yeast drying process. *IEEE Transactions on Neural Networks*, *19*(7), 1231–1242.

Zarrad, W., Harmand, J., Devisscher, M., & Steyer, J. P. (2004). Comparison of advanced control strategies for improving the monitoring of activated sludge processes. *Control Engineering Practice*, *12*(3), 323–333.

Zhang, X., & Hoo, K. A. (2008). Controlling a coupled set of biological reactors for wastewater treatment. *Control Engineering Practice*, *16*(5), 553–568.